Jul 5th, 12:00 AM - Jul 8th, 12:00 AM

Laboratory Experiments on Long Waves Interacting with Rigid Vertical Cylinders

R. Basile
Polytechnic University of Bari, rosangela.basile@poliba.it

F. De Serio
Polytechnic University of Bari

D. Raffaele
Polytechnic University of Bari

Laboratory experiments on long waves interacting with rigid vertical cylinders

R. Basile[1], F. De Serio[1] and D. Raffaele[1]
[1] DICATECh, Department of Civil, Environmental, Land, Building Engineering and Chemistry
Polytechnic University of Bari
Bari BA 70125
ITALY
E-mail: rosangela.basile@poliba.it

Abstract: *The impact of waves caused by storm surges or floods could lead to significant damage to marine and fluvial structures. Hydraulic forces add significant hydrodynamic loads on bridges built in coastal and fluvial environments; therefore, the effect of the wave impact on bridge substructures must be properly considered for the safe and cost-effective design of the piers. The use of laboratory-scale models is a direct approach to investigate the effects of long waves on simple structures, mimicking bridge piers. The present study describes a laboratory-scale model, where the propagation of two different long waves in a flume, in the presence of two rigid cylinders, was investigated. The velocity measurements were acquired by the Particle Image Velocimetry (PIV) technique, providing instantaneous flow velocity vectors on 2D planes. For each experimental condition, the instantaneous velocity field close to the cylinders was analysed, in order i) to depict how it changes during the wave transit, and thus how the drag force acting on the cylinders could change, ii) to detect the spatial distributions of vorticity downstream. Some first interesting results have been obtained, showing a quite uniform distribution of the longitudinal velocity along the depth of the vertical plane upstream of the cylinders, with increasing values during the wave transit. No interactions in the central part of the flow downstream of the two cylinders was observed in the horizontal plane which are spaced approximately ten times their diameter. Finally, the vorticity has also been studied, displaying a phase-varying behaviour, which appears to lose symmetry during wave transit.*

Keywords: Long waves, wave-structure interaction, particle image velocimetry, velocity distribution, vorticity.

1. INTRODUCTION

In the fluvial and marine environment, fundamental civil infrastructures like bridges, are often exposed to serious environmental loads, in particular when subjected to wave impacts. The extent of the damage caused by extreme waves in bridge substructures suggests that wave forces were not adequately considered in the design of piers. Therefore, in recent years there has been considerable interest in the safety of such facilities in extreme wave conditions. Research on wave forces acting on the bridge pier is essential for structural design and for the investigation of bridge failure mechanisms.

The use of laboratory-scale models is a direct and effective approach to investigate the effects of long waves on simple structures. A certain amount of past literature focused on experimental studies of different kinds of waves impacting on a vertical cylinder. Antolloni et al. (2020) discussed experimental results of long and moderately long wave-induced vortex generation around a slender vertical cylinder, obtained from velocity flow measurements acquired using the Particle Image Velocimetry (PIV) technique. The results showed that vortex formation occurring in the long waves is attached to the cylinder in the form of thin vortex tubes which appear symmetrically at angles of 40º-45º off the wave propagation direction. Vested et al. (2020) performed an experimental study with the combined use of PIV and Laser Doppler Velocimetry in order to investigate the force distribution on a vertical circular cylinder exposed to shoaling regular waves. The force distribution was measured for twenty regular wave conditions and in all cases it was found that the maximum force did not occur simultaneously on the individual sections of the cylinder. Li et al. (2012) performed a wave basin experiment to examine the interactions between multi-directional focused waves and a vertical bottom-mounted cylinder, proving that the focused run-up is directly proportional to the wave parameters including wave steepness, frequency bandwidth, and the directional spreading index. Wei et al. (2018) performed an experiment to investigate the dynamic responses of a bridge tower subjected to ocean waves and wave-

currents. Wave-induced base shear forces on the pile-group foundation and motion responses of the tower were analysed and the results showed that when a wave period is close to the natural period of the structure, an obvious resonance is induced on the structure. Furthermore, the longitudinal incident waves induced the largest longitudinal base shear forces on the foundation and the greatest dynamic motions on the upper tower of the structure. Mo et al. (2013) presented an experimental study of plunging solitary waves on a plane slope, with and without the interference of a vertical cylinder, using the PIV technique to record the time history of free surface elevations and temporal and spatial velocity variations in two fields of view.

Recent studies also focused on the flow behaviour around multi-cylinder structures, considered as obstacles necessary to mitigate the wave action. Tognin et al. (2019) exposed a peculiar experimental setup, designed to investigate the interaction between solitary waves and rigid emergent small-diameters cylinders representing rigid vegetation. Here it was observed observing that the cylinders strongly reduce the wave height based on their density.

The purpose of the present work is to describe a small-scale experiment representative of the propagation of long waves (such as for example flood waves due to heavy rains) on bridge piers. The experimental model reproduces the propagation of two long waves in a flume, in the presence of two rigid vertical cylinders simulating the bridge's piers. The velocity measurements are obtained with the use of the PIV technique, measuring instantaneous flow velocity vectors on different 2D planes. Specifically, the experiments consisted of flow velocity measurements: i) along the longitudinal plane of symmetry of both the cylinders, assessed upstream and downstream of each structure, and ii) on the horizontal plane at a specific distance from the flume bottom. Two solitary waves were released in the channel, overlapped on a uniform base flow, characterized by different values of flow rate, height, and period.

The aim of the present study is to provide some new benchmark data to improve the understanding of i) the time-varying vertical distribution of the drag and inertia forces acting on the cylinder during the wave transit, based on detailed measurements of the velocity distribution, ii) the time-varying velocity and vorticity field downstream of the cylinder in the horizontal plane.

2. EXPERIMENTAL SETUP

The experiments were performed at the Hydraulic Laboratory of the Polytechnic University of Bari (Italy). The rectangular flume, having a length of 25 m and a width of 0.4 m, was characterized by sidewalls and bottom constructed from Plexiglass which was well suited for optical measurements (see Figure 1).

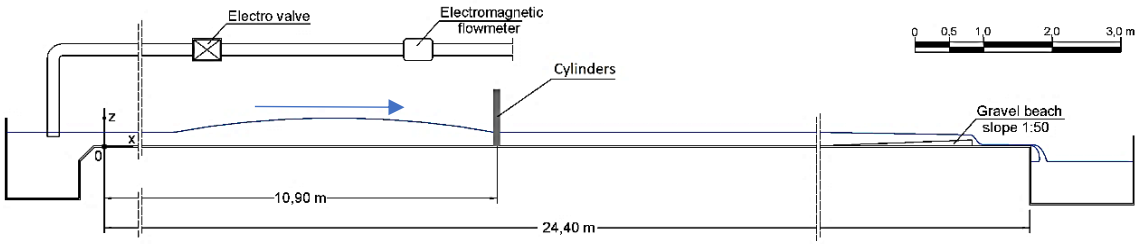

Figure 1 – Side view of the experimental setup, with the position of the cylinders.

The head tank could be fed by both a low-pressure and a high-pressure water circuit. The low-pressure main circuit provided constant flow conditions in the flume. The secondary high-pressure adduction pipe could release an additional water discharge in the head tank, controlled by an electronic actuated valve managed by a process PC with LabVIEW software. In this way, by properly tuning the added water release, the desired wave was generated in the channel, superimposed on the base flow.

At the downstream end of the channel, a secondary tank was located to receive the discharged flow. This was equipped with a triangular sharp-crested weir used to estimate the steady flow rate. The water level was controlled by a sloping gate at the end of the flume. In order to reduce the reflection of the generated waves, a structure with a high degree of porosity, consisting of a 2 m length metal cage with a 1 cm mesh filled with d_{50} = 1.50 cm gravel, was positioned on the bottom of the final part of the flume.

However, the measurements of the tested waves impinging on the model were acquired in a time period specifically chosen to avoid any reflection.

The model was designed according to Froude similitude, using a length scale factor equal to 1/10 (model/prototype). In this way we could evaluate the target phenomenon consistently with the lab available spaces. The experimental facility (Figure 1) consisted of two rigid cylinders having a diameter d = 20 mm, located along the y axis of the same transversal section, at a distance of x = 10.9 m from the header tank (being x the longitudinal axis of symmetry of the channel). They are positioned at equal distanced from the x axis, with y = 100 mm and y = -100 mm, respectively (Figure 2).

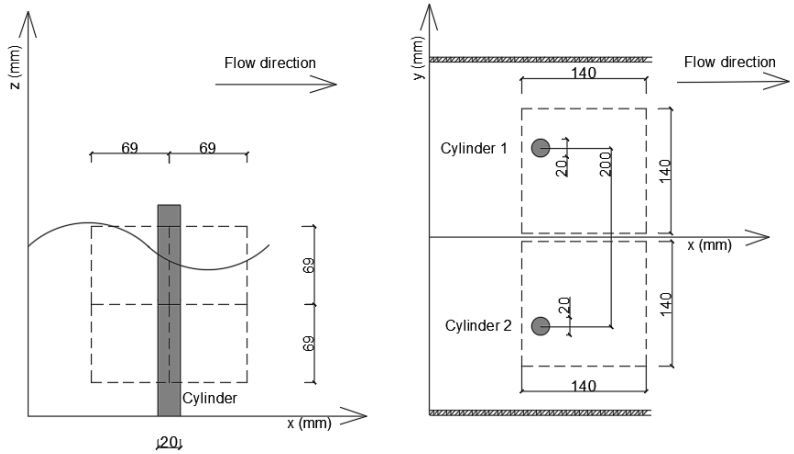

Figure 2 – Sketch illustrating the positions of the FoVs, in side-view (xz) on the left and plan-view (xy) on the right.

In order to obtain the flow velocity vectors on selected 2D planes, the velocity measurements were acquired by a PIV technique. The 2D PIV system was equipped with a FlowSense EO 4M-32 camera, a Bernoulli Laser (pulse energy of 200 mJ at 15 Hz) and a synchronizer controlled and monitored using a computer. The system was handled in double-frame mode, where the sampling frequency was settled to 13 Hz and the time interval between two frames of the same pair was 150 µs.

The data examined in the present work refers to the flow velocity measured in the horizontal plane (x,y) located at z = 30 mm from the bottom of the flume and containing both the cylinders, and in the longitudinal plane (x,z) passing through the centre of the first cylinder (located at y = -100mm).

In the horizontal plane, two field of views (FoVs) were properly selected (see Figure 2), each one containing a cylinder respectively. In the vertical plane, four FoVs were chosen: two filming below the free surface of the steady flow upstream and downstream of the cylinder respectively, and the other two filming in the upper part, to detect the passage of the solitary wave, again both upstream and downstream of the cylinder. In the present study, only data in the vertical plane upstream of the cylinder are shown for the sake of brevity.

After calibration, the obtained PIV images in the vertical plane had dimensions 69 × 69 mm, while the PIV images in the horizontal plane had dimensions 140 x 140 mm. The interrogation area of the images during adaptive correlation processing was 16×16 pixels; thus, the velocity vectors were assessed on points regularly spaced and distant 0.4 mm in the vertical plane and 0.8 mm in the horizontal plane, providing a very high spatial resolution.

The water depth in the flume was set to be 10.3 cm and the base flow rate, calculated using the flow rate scale for the Thomson-type triangular weir placed on the secondary tank, was 2.45 l/s.

In order to replicate, as an example, a flood propagation, two solitary waves, named O908 and O909, were used in the experiments. Each one was generated by linearly opening and successively closing the actuated valve of the high-pressure circuit for 19 s and 31 s (operating on a command PC in the Labview environment). Consequently, setting the maximum valve opening percentage to 70% for O908 and to 80% for O909, they had a wave height of 2.5 cm and 5 cm respectively and a wave period T = 20,000 ms.

The number of images acquired by PIV was limited by technical reasons related to storage size; therefore, the number of images per measurement was set to 150t. Consequently, the total acquisition time for each measurement was equal to 18,400 ms, that is lower than the entire wave period. Nevertheless, this was sufficient to capture the ascending and descending phase of both waves.

3. EXPERIMENTAL RESULTS AND DISCUSSION

The stationary conditions in the channel, typical of the base flow, i.e., the one characterized by h = 10.3 cm and q = 2.45 l/s, provided a reference average velocity equal to u_0 = 0.06 m/s. By setting the kinematic viscosity $\nu = 10^{-9}$ m^2/s, the flow Reynolds number was Re_f = 24000 and therefore the flow in the channel was turbulent. We also calculated the cylinder Reynolds number, $Re_{cyl} = u_0 * d/\nu$ = 1200, suggesting the presence of a laminar boundary layer on the cylinder front and a detachment of alternating vortices downstream it (Kirkil et al., 2015; Maraglino et al., 2019).

To evaluate the velocity vector field from pairs of particle images, the adaptive correlation method was used as first step of data processing. The resulting vector maps were examined and used also to extract the vorticity maps. Firstly, and for both O908 and O909 waves, the analysis focused on the vertical plane upstream of the cylinder (FoVs in Figure 2). The flow field was observed both in stationary conditions and in wave conditions, while varying during the passage of the long wave. Considering that the u velocity and the wave elevation are in phase, in Figure 3 the time series of the u horizontal velocity in a selected point close to the cylinder (located at x=10.87m and z=0.03m) is shown. In this graph, some specific values t/T are highlighted by a red line, referring respectively to the trough wave condition (*P1*), the peak of the wave (*P2*), two values (equi-spaced) in the descending phase of the wave (*P3, P4*) and the final value, approaching again the wave trough (*P5*).

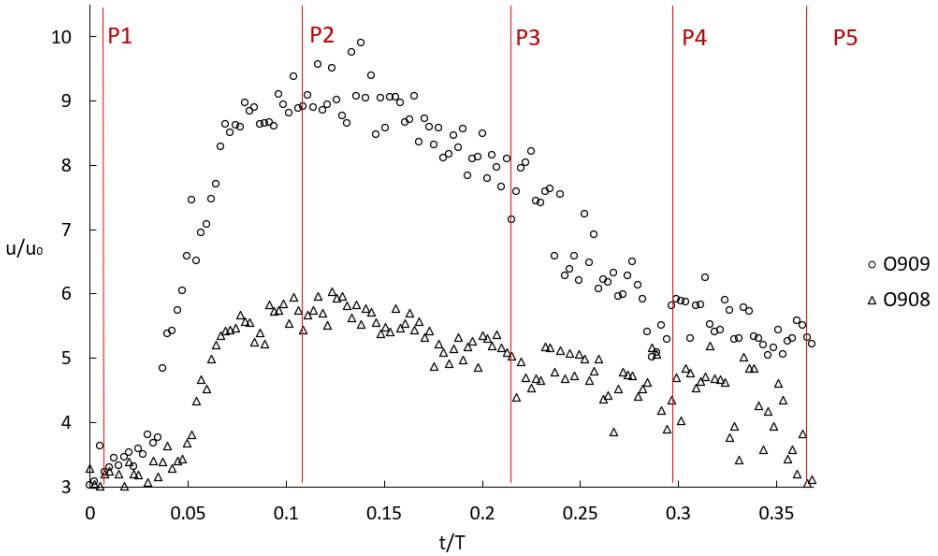

Figure 3 - Longitudinal velocity time series relative to point *Q* during the propagation of the waves.

The vertical profiles of u were extracted for each instant time mentioned above, at the selected point located at x = 10.87 m. Figure 4 displays the comparison between these five vertical velocity profiles of u, normalized by the average velocity u_0, for both the examined waves. The vertical profiles along z/h have been obtained by merging the instantaneous velocity maps of the two FoVs (upper and lower, as in Figure 2). In particular, for the O908 wave, the FoVs capture the image of the cylinder at 2 cm from the bottom of the flume, while for the O909 wave, the FoVs capture it at 4.5 cm from the bottom of the flume, in order to detect the entire height of the wave. It is evident that all the vertical profiles have a quite flat vertical trend, meaning that the distribution of the u velocity is quite uniform along the depth. Rather, we observe increasing values of u/u_0 due to the wave transit, which reach a maximum at the wave peak, as expected (u/u_0 = 6.15 for O908 and u/u_0 = 9.3 for O909). Moreover, the transit of the wave is evidently proved also by the increased relative heights z/h where the velocities are detected, with respect to z/h, close to 0.9 in the P1 profile. For the wave O908, a maximum relative wave height

z/h = 1.13 is reached in P2, while for wave O909, the maximum relative height in P2 is *z/h* = 1.3. Coherently with the descending branch of the wave, P3, P4 and P5 profiles show lower velocities and heights gradually. The P3, P4 and P5 profiles for the O908 wave have similar u/u_0 velocity values, being the descending branch of the time series (Figure 3) less sloped than for the O909 wave.

Knowing the distribution of the longitudinal components of the longitudinal velocity *u* in both wave conditions, may allow us to detect the force acting on the cylinder per unit height. In fact, expressions like the Morison's equation can be adopted in this case, considering the sum of the inertia and drag contributions (1):

$$F(t) = C_M \rho \frac{\pi d^2}{4} \frac{du}{dt} + C_D \frac{1}{2} \rho du|u| \qquad (1)$$

where ρ is the water density, C_D is the drag coefficient and C_M is the inertia coefficient (both can be assumed ~ 1 in our case). It is evident that in the case of the O909 wave, the cylinder is expected to be affected by higher force values e than in the case of the O908 wave, due to the higher *u* peak velocity and greater variation in the time period of the *u* velocity.

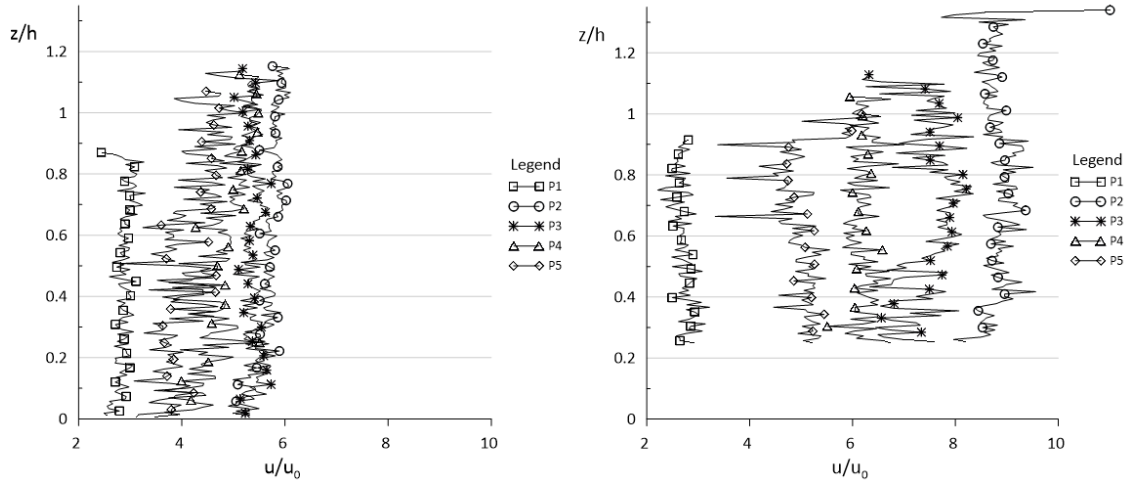

Figures 4 - Comparison between the vertical profiles of the longitudinal velocity *u* normalized by the average velocity u_0, as measured at five instant times related to wave trough: (P1), wave peak (P2), descending wave (P3 and P4), approaching trough (P5) for (a) wave O908 and (b) wave O909.

As a second step, the results obtained from the FoVs in the horizontal plane, at *z* = 0.03 m, downstream of the two cylinders (Figure 2) were analysed for both O909 and O908 waves. In this case we chose four instant times as been significant to describe the wave behaviour such as wave trough, ascending branch, wave peak and descending branch.

For the O908 wave, Figure 5 shows the instantaneous velocity horizontal maps in the two selected FoVs, each one containing a cylinder respectively, during the wave transit. The analogous plot is shown in Figure 6 for the O909 wave. In such plots the reference system used refers to the frame (x_f, y_f). It is necessary to point out the presence of a shaded region up to x_f = 40 mm, due to the shadow caused by the laser light source on the two cylinders. It is evident that, being the two cylinders spaced along *y* ~ 10d, no interaction is observed in the central part of the flow, which remains quite undisturbed.

The horizontal velocity vectors (having components *u* along *x*, and *v* along *y*) gradually increase from 0.1 m/s to 0.4 m/s for the O908 wave and up to 0.5 m/s for the O909 wave, while going from the trough condition to the peak one. This is observed generally in points far from the wake of the cylinder. Figures 5 and 6 in fact highlight the presence of a wake behind the cylinders, where the velocity magnitude abruptly decreases (up to values from 0 m/s to 0.1 m/s) as expected and where a detachment of eddies occurs.
To evaluate the vorticity W_z, we have computed the vorticity maps, plotted in Figure 7 and 8 respectively for O908 and O909 waves, always for the selected four instant times. For the case of the wave trough, opposite values of vorticity are observed (and quite symmetrical) downstream of each cylinder: anticlockwise (negative) on the left side of the cylinder wake and clockwise (positive) on the right side.

This is consistent with the stationary case of a flow impacting a cylinder. During the three successive time steps (ascending, peak, descending) the symmetry seems lost, and the negative vorticity affects also the right side, while the positive vorticity spreads more downstream. In the peak condition, the most intense vorticity values are observed with values in the range from W_z = -0.1 s^{-1} to W_z = 0.1 s^{-1} for O908 wave and in the range from W_z = -0.2 s^{-1} to W_z = 0.2 s^{-1} for O909 wave.

Finally, we have examined how the presence of the two cylinders influences the velocity distribution in the transverse direction. Figures 9 and 10 illustrate the transverse profiles of the longitudinal *u* velocity during the trough, the ascending branch, the peak and the descending branch for the O908 and O909 waves. For each profile, the *u* velocity is normalized by its maximum value U_{max} measured along the profile itself. Moreover, we compare the transversal profiles at five different positions, at increasing distances from the cylinders (x_f = 50.4 mm, x_f = 70.4 mm, x_f = 90.4 mm, x_f = 110.4 mm, x_f = 130.4 mm).

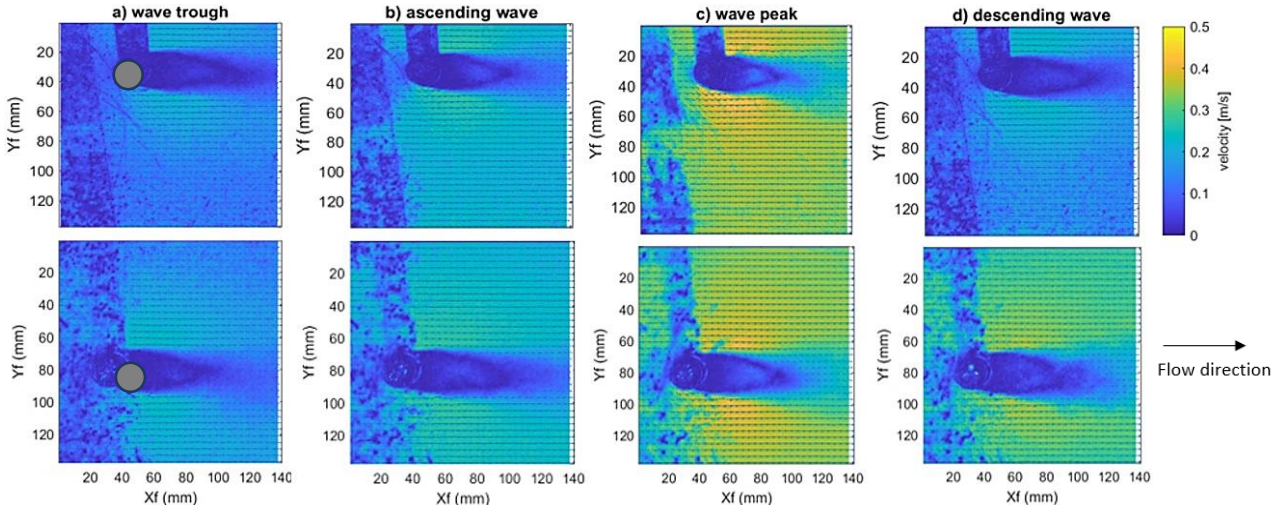

Figures 5 - The velocity in the horizontal plane during the wave transit: (a) trough, (b) ascending phase, (c)peak and (d) descending phase of O908 wave.

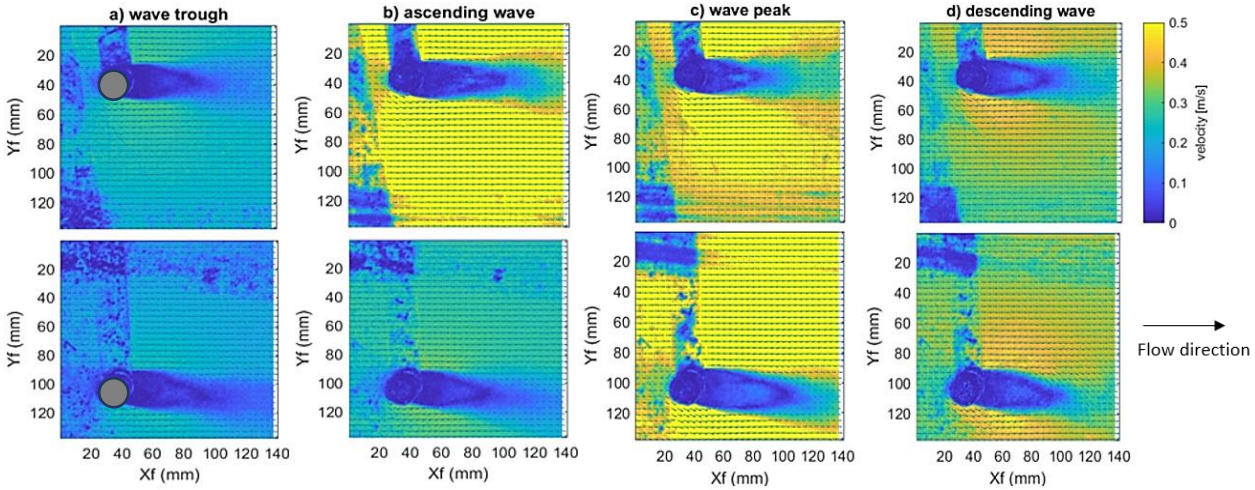

Figures 6 - The velocity in the horizontal plane during the wave transit: (a) trough, (b) ascending (c) phase, peak and (d) descending phase of O909 wave.

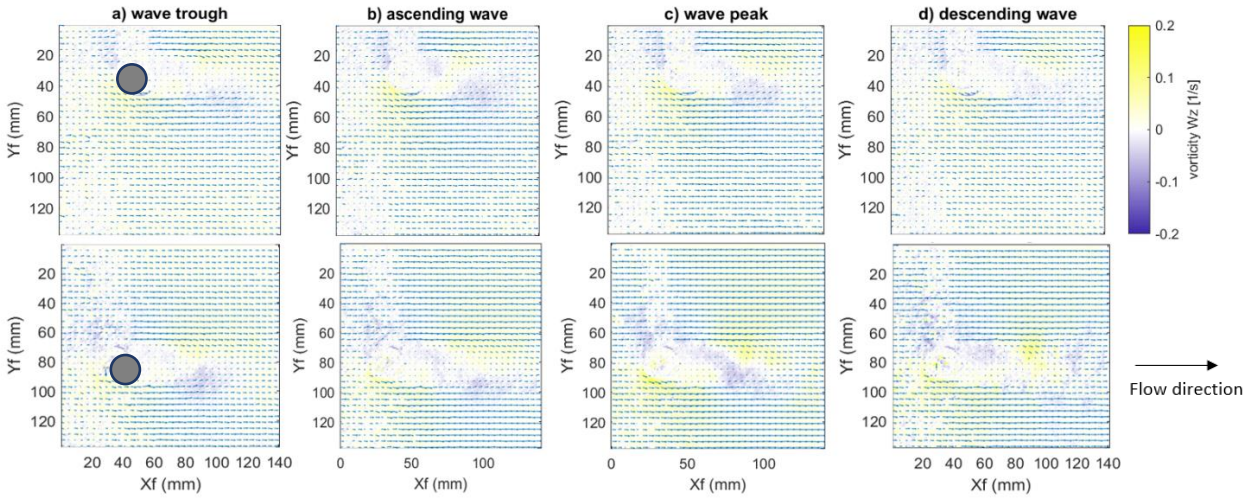

Figures 7 - Vorticity in the horizontal plane during the wave transit: (a) trough, (b) ascending phase, (c) peak and (d) descending phase of O908 wave.

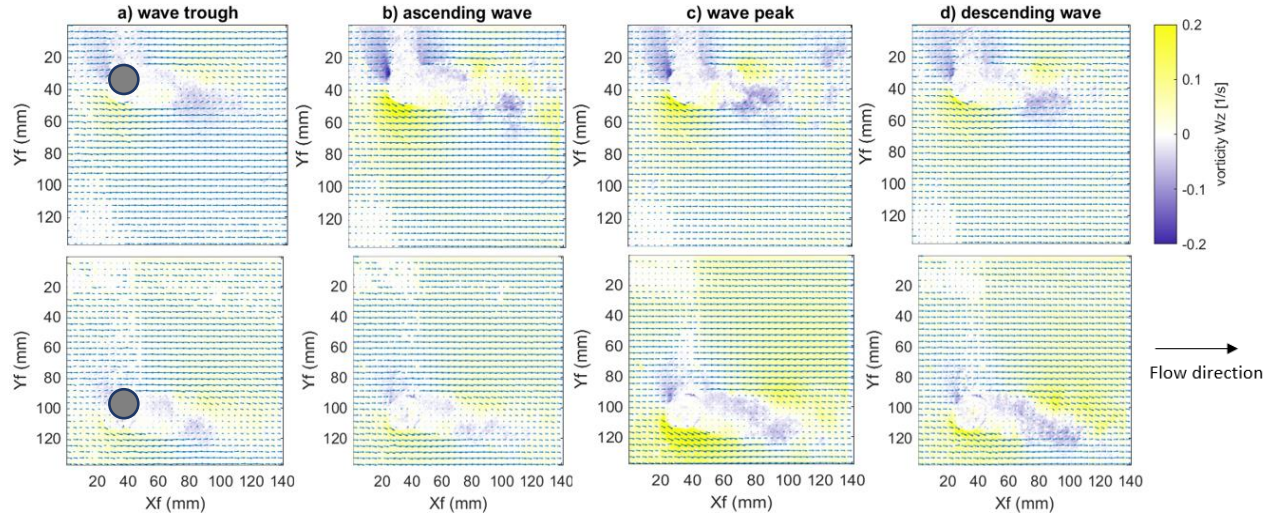

Figures 8 - Vorticity in the horizontal plane during the wave transit: (a) trough, (b) ascending phase, (c) peak and (d) descending phase of O909 wave.

At the same distance from the cylinders, the transversal profiles of the two waves show a similar trend, meaning that in the region between the two cylinders and outside the wake, the velocity is quite uniform with a magnitude of approximately 80% of the maximum value. A relevant velocity reduction is noted downstream of the cylinders, passing from u/U_{max} = 0.6 to u/U_{max} = 0.01 in the case of the wave O908 in x_f = 50.4 mm, and from u/U_{max} = 0.7 to u/U_{max} = -0.2 in the case of the wave O909, at the same distance.

When a negative sign is observed for u/U_{max}, the presence of a vortex should be assumed. With increasing x_f distances, the velocity in the cylinders' wakes gradually increase tending to represent the original base flow.

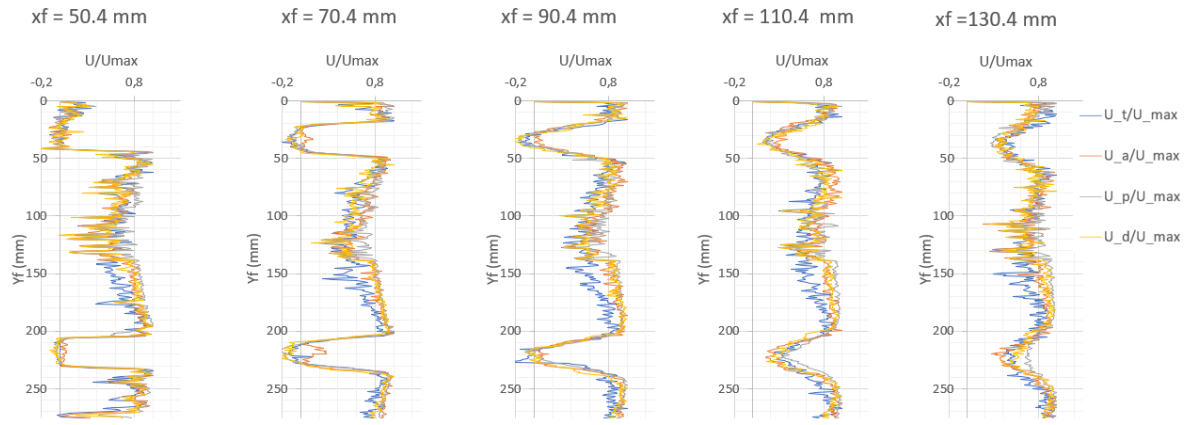

Figures 9 – Transverse profiles during the trough, the ascending branch, the peak and the descending branch of O908 wave, at selected distances x_f.

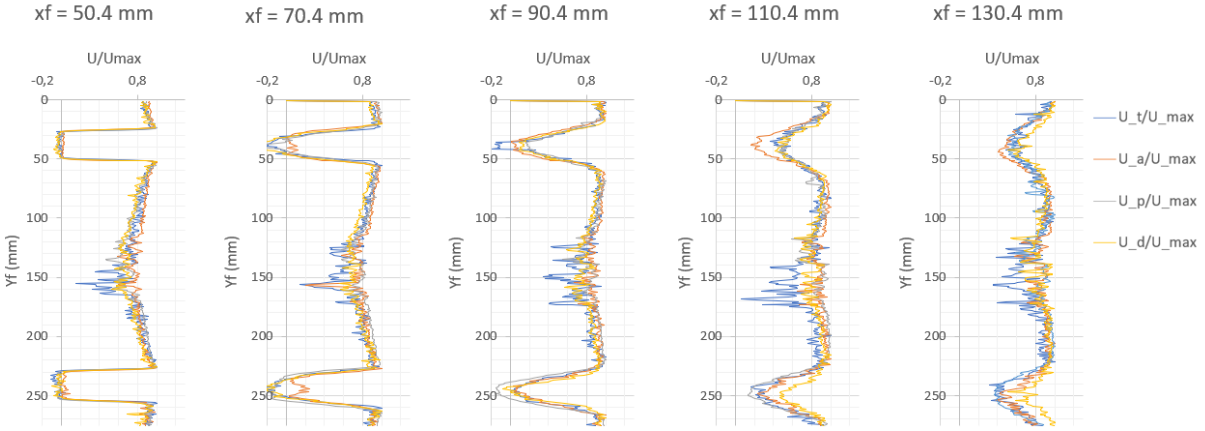

Figures 10 – Transverse profiles during the trough, the ascending branch, the peak and the descending branch of O909 wave, at selected distances x_f

4. CONCLUSION

This study describes a laboratory-scale model, where the propagation of two different long waves in a flume in presence of two rigid cylinders, mimicking bridge piers, is investigated using Froude similtude. The velocity measurements acquired by the PIV technique have provided the following results.

The vertical profiles of the longitudinal velocity u upstream of each cylinder, normalized by the average velocity u_0, for both the examined waves, show a quite flat vertical trend, meaning that the distribution of the u velocity is quite uniform along the depth. Increasing values of u/u_0 are observed due to the wave transit, reaching a maximum at the wave peak, as expected (u/u_0= 6.15 for O908 and u/u_0 = 9.3 for O909). Furthermore, the presence of the wave transit is evident also from the increased relative heights z/h at the position where the velocities are detected.

Downstream of both cylinders, the velocities in the horizontal plane at the transverse distance of ~10d between the two cylinders highlights that no interactions are observed in the central part of the flow which remains quite undisturbed. In points far from the cylinders' wakes, the horizontal velocity gradually increases from 0.1 m/s to 0.4 m/s for the O908 wave and up to 0.5 m/s for the O909 wave, during their transits. In the wakes behind the cylinders, the velocity abruptly decreases as expected and a detachment of vortices occurs. During the wave trough, opposite values of vorticity are observed, and which are quite symmetrical downstream of each cylinder. During the three successive examined time steps, the symmetry seems to reduce, and the negative vorticity prevails close to the cylinders, while the positive vorticity spreads further downstream.

The velocity distribution in the transverse direction observed at five different positions, shows a similar trend at the same distance from the cylinders for both waves, meaning that in the region between the two cylinders and outside the wake the velocity, is quite uniform generally around 80% of the maximum value. With increasing distances from the cylinders, the velocity in the cylinders' wakes gradually increase, tending to re-establish the original flow.

5. REFERENCES

1. Antolloni, G., Jensen, A., Grue, J., Riise, B. and Brocchini, M. (2020), *Wave-induced vortex generation around a slender vertical cylinder,* Physics of Fluids, 32, 1-10
2. Bradner, C., Schumacher, T., Cox, D. and Higgins, C. (2011), *Experimental setup for a large-scale Bridge superstructure model subjected to waves*, Journal of waterway, port, coastal and ocean engineering, 137, 3-11
3. Chella, M.A., Bihs, H., Myrhaug, D. and Muskulus, M. (2017), Breaking solitary waves and breaking wave forces on a vertically mounted slender cylinder over an impermeable sloping seabed, J. Ocean Eng. Mar. Energy, 3, 1-19
4. Guo, A., Liu, J., Chen, W., Bai, X., Liu, G., Liu, T., Chen, S. and Li, H. (2016), *Experimental study on the dynamic responses of a freestanding bridge tower subjected to coupled actions of wind and wave loads*, Journal of wind engineering and industrial aerodynamics, 159, 36-47
5. Kirkil, G. and Constantinescu, G. (2015), *Effects of cylinder Reynolds number on the turbulent horseshoe vortex system and near wake of a surface-mounted circular cylinder*, Physics of Fluids, 27, 1-25
6. Li, J., Wang, Z. and Liu, S. (2012), *Experimental study of interaction between multi-directional focused wave and vertical circular cylinder, part I: Wave run-up*, Coastal Engineering, 64, 151-160
7. Li, J., Wang, Z. and Liu, S. (2014), *Experimental study of interaction between multi-directional focused wave and vertical circular cylinder, part II: Wave force*, Coastal Engineering, 83, 233-242
8. Liu, C., Zhang, S. and Hao, E. (2017), *Joint earthquake, wave and current action on the pile group cable-stayed bridge tower foundation: an experimental study*, Applied Ocean Research, 63, 157-169
9. Malavasi, S. and Guadagnini, A. (2003), *Hydrodynamic Loading on River Bridges*, Journal of Hydraulic Engineering, 129, 854-861
10. Maraglino, D., Meftah, M.B., De Serio, F., Mossa, M. (2019), *Fields measurements in a flow around a hydrofoil: some preliminary results*, in International Workshop on Metrology for the Sea, Genoa, October 3-5, 2019, pp. 270-275
11. Mo, W., Jensen, A. and Liu, P. (2013), *Plunging solitary wave and its interaction with a slender cylinder on a sloping beach*, Ocean Engineering, 74, 48-60
12. Park, H., Tomiczek, T., Cox, D.T., van de Lindt, J. W. and Lomonaco, P. (2017), *Experimental modeling of horizontal and vertical forces on an elevated coastal structure*, Coastal Engineering, 128, 58-74
13. Seiffert, B., Hayatdavoodi, M. and Ertekin, R.C. (2014), *Experiments and computations of solitary-wave forces on a coastal-bridge deck, part I: Flat Plate*, Coastal Engineering, 88, 194-209
14. Tognin, D., Peruzzo, P., De Serio, F., Meftah, M.B., Carniello, L., Defina, A. and Mossa, M. (2019), *Experimental setup and measuring system to study solitary wave interaction with rigid emergent vegetation*, Sensors, 19
15. Vested, M. H., Carstensen, S. and Christensen, E. D. (2020), *Experimental study of wave kinematics and wave load distribution on a vertical circular cylinder*, Coastal Engeneering, 157, 1-18
16. Wei, C., Zhou, D. and Ou, J. (2018), *Wave and wave-current actions on a bridge tower: an experimental study*, Advanced in Structural Engineering, 1-12
17. Zhu, D. and Dong, Y. (2020), *Experimental and 3D numerical investigation of solitary wave forces on coastal bridges*, Ocean Engineering, 2019, 1-15